

DFT and TD-DFT studies on symmetrical squaraine dyes for nanocrystalline solar cells

Jie Xu · Hui Zhang · Lei Wang · Guijie Liang ·
Luoxin Wang · Xiaolin Shen · Weilin Xu

Received: 1 December 2009 / Accepted: 16 March 2010 / Published online: 9 April 2010
© Springer-Verlag 2010

Abstract The ground-state geometries, electronic structures, and electronic absorption spectra of symmetrical squaraine dyes SQ1–SQ4 were investigated using density functional theory and time-dependent DFT at the B3LYP level. The calculated geometries indicate that strong conjugation effects occur in the dyes. The highest occupied molecular orbital energy levels were calculated to be –4.95, –5.22, –5.09, and –5.06 eV, and the lowest unoccupied molecular orbital energies were –2.72, –3.05, –2.80, and –2.80 eV for SQ1–SQ4, respectively. Taking the conduction band energy of TiO₂ into account, these data reveal the sensitized mechanism: the interfacial electron transfer between the semiconductor TiO₂ electrode and the dye sensitizers SQ1–SQ4 are electron-injection processes from excited dyes to the semiconductor conduction band. The intense calculated absorption bands are assigned to $\pi \rightarrow \pi^*$ transitions, which exhibit appreciable blue-shift compared with the experimental absorption maxima due to the inherent approximations in the TD-DFT.

Keywords Density functional theory · Squaraine dyes · Dye-sensitized solar cells · Electronic structures · Absorption spectra

Introduction

Increasingly serious energy-demanding and environment-related new energy systems based on renewable sources are attracting increasing attention. Over recent years, significant emphasis has been put on the development and understanding of light-driven charge separation in molecular systems as methods of converting and storing solar energy. Dye-sensitized solar cells (DSSCs) have attracted widespread interest for conversion of sunlight into electricity, because of their high efficiency and low cost [1–5]. The most efficient sensitizers employed in these cells are ruthenium polypyridyl complexes, yielding solar-to-electric power conversion efficiencies up to 10–11% under AM 1.5 [4]. However, the ruthenium complexes are unable to make full use of the solar spectrum because of their lack of absorption in the far-red/near-IR region. Therefore, great effort should be made to develop dye sensitizers with extended absorption and spectral sensitivity into the far-red/near-IR region.

Squaraines are well-known for their extremely high extinction coefficients, inherent stability, and intense absorption in the far-red/near-IR region, which make them attractive for solar cell applications. The ability of squaraines to act as sensitizers for large-bandgap oxide semiconductors has been investigated by several groups [6–12]. Initial tests showed that commercial squaraines were capable of electron injection into TiO₂, but IPCE values of only 4–10% were obtained because of the lack of any anchoring groups in these molecules. Recently, symmetrical anilino-squaraines (SQ1–SQ4) containing short carboxyl anchoring groups were designed and synthesized, yielding a maximum monochromatic incident photon-to-current conversion efficiency of 73% at 670 nm [8].

An accepted model for DSSC is as follows: a sensitizing dye molecule absorbs visible or near infrared light and

J. Xu (✉) · H. Zhang · L. Wang · L. Wang · X. Shen · W. Xu
Key Lab of Green Processing and Functional Textiles of New
Textile Materials, Ministry of Education,
Wuhan University of Science and Engineering,
Wuhan 430073, China
e-mail: xujie0@ustc.edu

G. Liang
College of Materials Science and Engineering,
Xi'an Jiao Tong University, Xi'an 710049, China

injects an electron into the semiconductor from its excited state(s) [13]. When the electron is transferred to the TiO₂ solid, it proceeds through the semiconductor to an external circuit. Subsequently, the oxidized sensitizer receives an electron from an electron donor, such as iodide ion, present in the electrolyte. Therefore, the performance of DSSC strongly depends upon the following factors:

- 1 the absorption efficiency of the sensitizing dye for the solar light spectrum;
- 2 the probability of electron transfer from the excited state of the sensitizing dye to TiO₂ (efficiency of the charge separation); and
- 3 the probability of electron transfer from the electron donor to the oxidized dye [3].

All these factors are closely associated with the structure of the ground and excited electronic states of the sensitizing dye. From this point of view, it is imperative to investigate the electronic structures of both ground and excited states of the sensitizing dye molecule to understand the mechanisms of charge separation and electron transfer, which are the key processes in this type of solar cell. In order to design and synthesize more efficient sensitizing dyes, it is also necessary to understand the electronic structures of the existing efficient sensitizing dyes.

Density functional theory (DFT) has emerged as a reliable standard tool for theoretical treatment of structures and electronic and absorption spectra. Its time-dependent extension called time-dependent DFT (TD-DFT) can give reliable values for valence excitation energies with the standard exchange–correlation functionals. The computational cost of TD-DFT calculation is comparable with that of a Hartree–Fock (HF)-based single excitation theory, for example configuration interaction singles (CIS) or the time-dependent HF (TD-HF) method, and maintains uniform accuracy for open-shell and closed-shell systems. In recent years, TD-DFT has been extensively used to study the structures and absorption spectra of dye sensitizers for DSSCs [4, 14–23]. In order to understand the sensitized mechanism, the geometries and electronic structures of the dye sensitizers SQ1–SQ4 were studied in detail using DFT, and the electronic absorption spectra were investigated by use of TD-DFT calculations in this work.

Results and discussion

Geometric structures

The anilino-squaraine dyes SQ1–SQ4 contain an electron-withdrawing central four-membered squaric ring, two electron-donating alkyls, and two short carboxyl anchoring groups in the form of donor–acceptor–donor (DAD). The

optimized ground-state geometries of the squaraine dyes SQ1–SQ4 are shown in Fig. 1, and selected bond lengths, bond angles, and dihedral angles are listed in Table 1. All the CC lengths in the squaric and the two phenyl rings are between the distance of a C–C single bond and a C=C double bond, implying there is extensive delocalization throughout the molecule. The phenyls serve as two conjugation bridges connecting the DAD system. The delocalization in the conjugation paths is beneficial to intramolecular charge transfer and to the stability of the molecule. The C=O bonds in the squaric rings of SQ2 and SQ4 are slightly shorter than those of SQ1 and SQ3, because the electron-donating ability of the long alkyl group (−C₄H₉) is stronger than that of the short alkyl group (−CH₃). All C–N bonds of SQ2 and SQ4 are longer than those of SQ1 and SQ3, and the dihedral angles C6–C1–N7–C8 of SQ2 and SQ4 are larger, which can be attributed to the greater steric hindrance of the long alkyl group. Moreover, the C6–C1–N7–C8 angle of SQ2 is much larger than those of SQ1, SQ3, and SQ4, indicating that the anilino groups of SQ2 are significantly distorted because of the largest steric hindrance from its long alkyl and carboxyl groups.

Electronic structures

Natural population analysis was used to characterize intramolecular charge transfer. The dipole moments for SQ1–SQ4 are 1.019, 2.987, 0.169, and 0.404, respectively, which are much lower than those of the indolines, because of the symmetrical structures of the squaraines present [23]. Table 2 lists the values of the quadrupole moments for SQ1–SQ4, where the average of the diagonal quadrupole moment tensor elements Q_{ii} and the unique quadrupole moment Q are defined as follows:

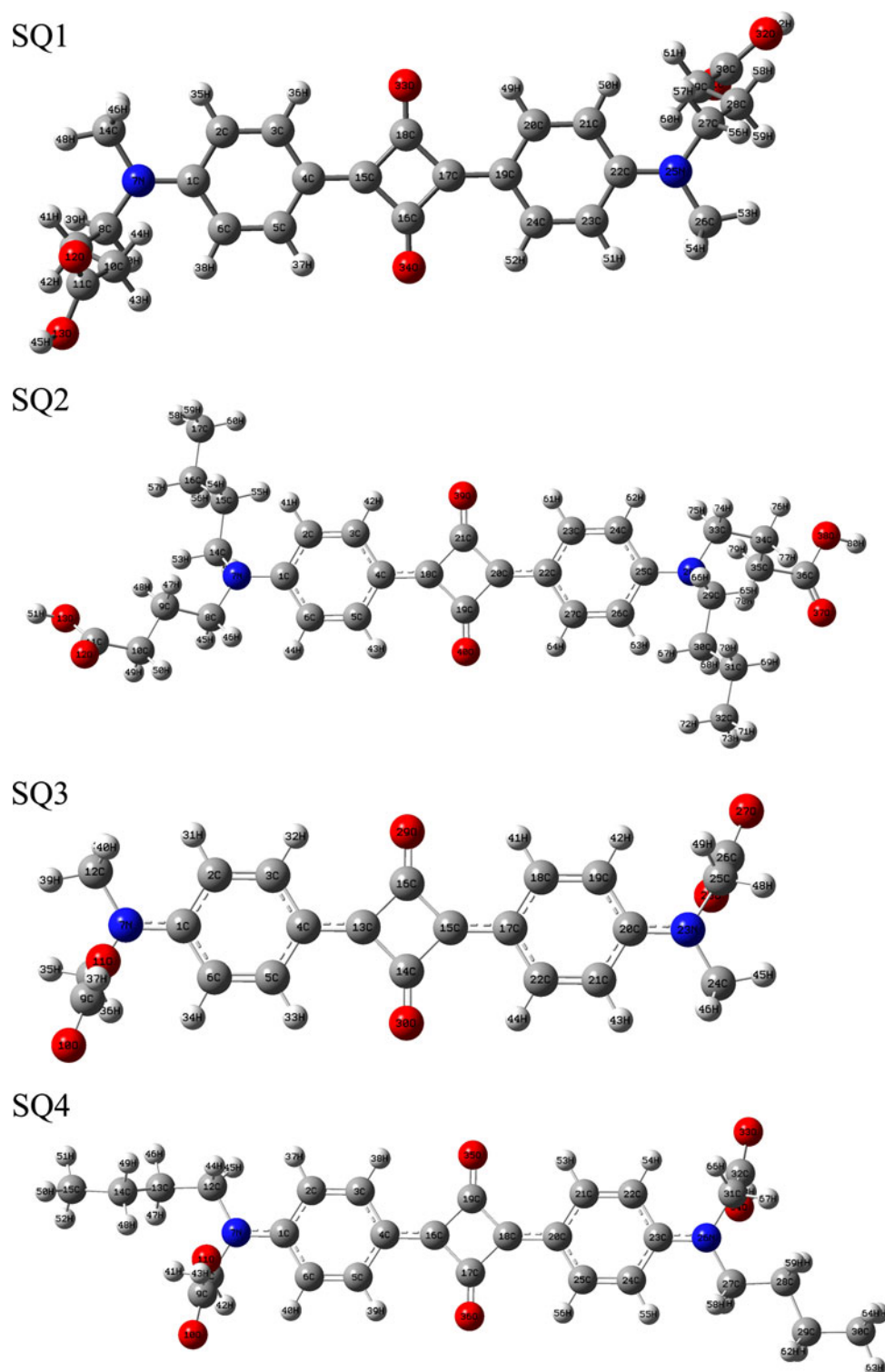
$$Q_{ii} = (Q_{XX} + Q_{YY} + Q_{ZZ})/3$$

$$Q = Q_{XX} - Q_{YY}.$$

All the diagonal elements of the quadrupole moment tensors for SQ1–SQ4 are negative, indicating that the negative charge distribution is farther removed from the molecular center of the nuclear charges. The off-diagonal tensor elements Q_{ij} vanish whenever the molecule has a plane of symmetry perpendicular to either of the coordinates i or j . As the squaraines were placed along the x -axis with C1 at the origin, the off-diagonal elements Q_{xy} and Q_{yz} of the squaraines vanish because of the C1-y-axis, as shown in Fig. 1.

The natural charges of the alkyl, aminocarboxyl, phenyl, and squaric groups in SQ1–SQ4 are summarized in Table 3. It is found that the alkyl and phenyl groups are electron-donor units whereas the aminocarboxyl and squaric groups are electron-acceptor units. The aminocarboxyl groups in SQ3 and SQ4 are more negative than

Fig. 1 Optimized ground-state geometries of the squaraine dyes SQ1–SQ4



those in SQ1 and SQ2, because of the stronger electron-withdrawing ability of short carboxyl group ($-\text{CH}_2\text{COOH}$) than long carboxyl group ($-(\text{CH}_2)_3\text{COOH}$). The negative charge of the squaric ring in SQ2 is much lower than that of SQ1, SQ3, and SQ4, indicating the weaker electron-withdrawing ability of the squaraine core in SQ2.

The frontier molecular orbital (MO) energies of the squaraine dyes SQ1–SQ4 are given in Fig. 2. For SQ1, the highest occupied MO (HOMO), lying at -4.95 eV, is delocalized throughout the dye, whereas the HOMO-1, 1.09 eV below the HOMO, is entirely localized within the squaraine core, both orbitals belonging to the dye π

Table 1 Selected bond lengths (\AA), bond angles ($^\circ$), and dihedral angles ($^\circ$) of the squaraine dyes SQ1–SQ4

SQ1	SQ2		SQ3		SQ4	
C1–C2	1.4289	C1–C2	1.4208	C1–C2	1.4259	C1–C2
C2–C3	1.3776	C2–C3	1.3795	C2–C3	1.3780	C2–C3
C4–C15	1.4101	C4–C18	1.4134	C4–C13	1.4108	C4–C16
C15–C16	1.4703	C18–C19	1.4730	C13–C14	1.4726	C16–C17
C16–O34	1.2372	C19–O40	1.2350	C14–O30	1.2365	C17–O36
C1–N7	1.3673	C1–N7	1.3981	C1–N7	1.3699	C1–N7
N7–C8	1.4670	N7–C8	1.4709	N7–C8	1.4496	N7–C8
N7–C14	1.4623	N7–C14	1.4843	N7–C12	1.4623	N7–C12
O34–C16–C15	135.2	O40–C19–C18	135.3	O30–C14–C13	135.2	O36–C17–C16
C16–C15–C18	90.3	C19–C18–C21	90.5	C14–C13–C16	90.4	C17–C16–C19
C15–C4–C5	121.3	C18–C4–C5	120.9	C13–C4–C5	121.2	C16–C4–C5
C6–C1–N7	122.6	C6–C1–N7	122.2	C6–C1–N7	121.7	C6–C1–N7
C6–C1–N7–C8	–4.9	C6–C1–N7–C8	23.1	C6–C1–N7–C8	1.6	C6–C1–N7–C8
C6–C1–N7–C14	178.8	C6–C1–N7–C14	–119.9	C6–C1–N7–C12	172.0	C6–C1–N7–C12
C5–C4–C15–C16	0.2	C5–C4–C18–C19	0.3	C5–C4–C13–C14	0.1	C5–C4–C16–C17
						0.8

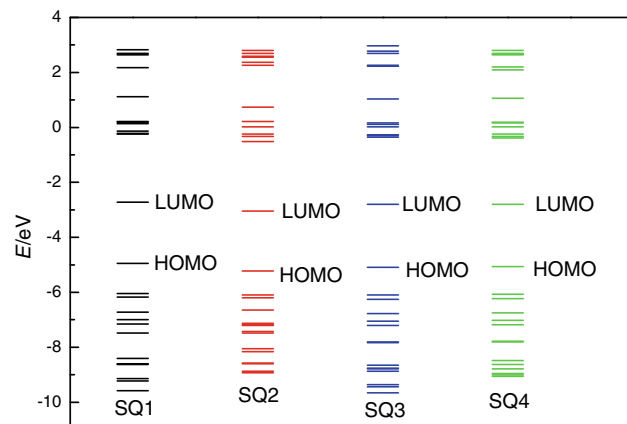
Table 2 Quadrupole moments of the squaraine dyes SQ1–SQ4

Dyes	Q_{xx}	Q_{yy}	Q_{zz}	Q_{xy}	Q_{xz}	Q_{yz}	Q_{ii}	Q
SQ1	–74.510	–203.979	–128.264	–45.093	93.509	–11.128	–135.584	129.469
SQ2	–140.743	–248.693	–204.661	–37.738	63.174	–15.389	–198.032	107.950
SQ3	–46.481	–156.747	–191.519	–4.300	44.836	–4.557	–131.582	110.266
SQ4	–69.061	–194.149	–219.289	13.114	67.372	7.953	–160.833	125.088

Table 3 Natural charges (e) of different groups in the squaraine dyes SQ1–SQ4

Dyes	Alkyl	Aminocarboxyl	Phenyl	Squaric
SQ1	0.215	–0.254	0.362	–0.694
SQ2	0.192	–0.297	0.384	–0.552
SQ3	0.221	–0.290	0.384	–0.632
SQ4	0.257	–0.320	0.377	–0.633

framework (Fig. 3). The lowest unoccupied MO (LUMO), 2.23 eV above the HOMO, is a π^* orbital delocalized throughout the dye, whereas the LUMO+1, 2.47 eV above the LUMO, is localized within the squaric and phenyl rings. For SQ2, the HOMO, lying at –5.22 eV, is delocalized throughout the dye. The HOMO–1, 0.87 eV below the HOMO, is also a π orbital delocalized throughout the dye whereas the HOMO–2, 0.98 eV below the HOMO, is a π orbital mainly localized within the squaraine core. The LUMO, 2.18 eV above the HOMO, is a π^* orbital delocalized throughout the dye and the LUMO+1, 2.53 eV above the LUMO, is localized throughout the dye. For SQ3, the HOMO, lying at –5.09 eV, is delocalized throughout the dye whereas the HOMO–1, 1.00 eV below the HOMO, is entirely localized in the squaraine core. The

**Fig. 2** Frontier molecular orbital energies of the squaraine dyes SQ1–SQ4

LUMO, 2.29 eV above the HOMO, is a π^* orbital delocalized throughout the dye, whereas the LUMO+1, 2.45 eV above the LUMO, is localized within the squaric and phenyl rings, with sizable contributions arising from the carboxylic group. For SQ4, the HOMO is lying at –5.06 eV and the LUMO is lying at –2.80 eV. The LUMO+1 consists of sizable contributions arising from the

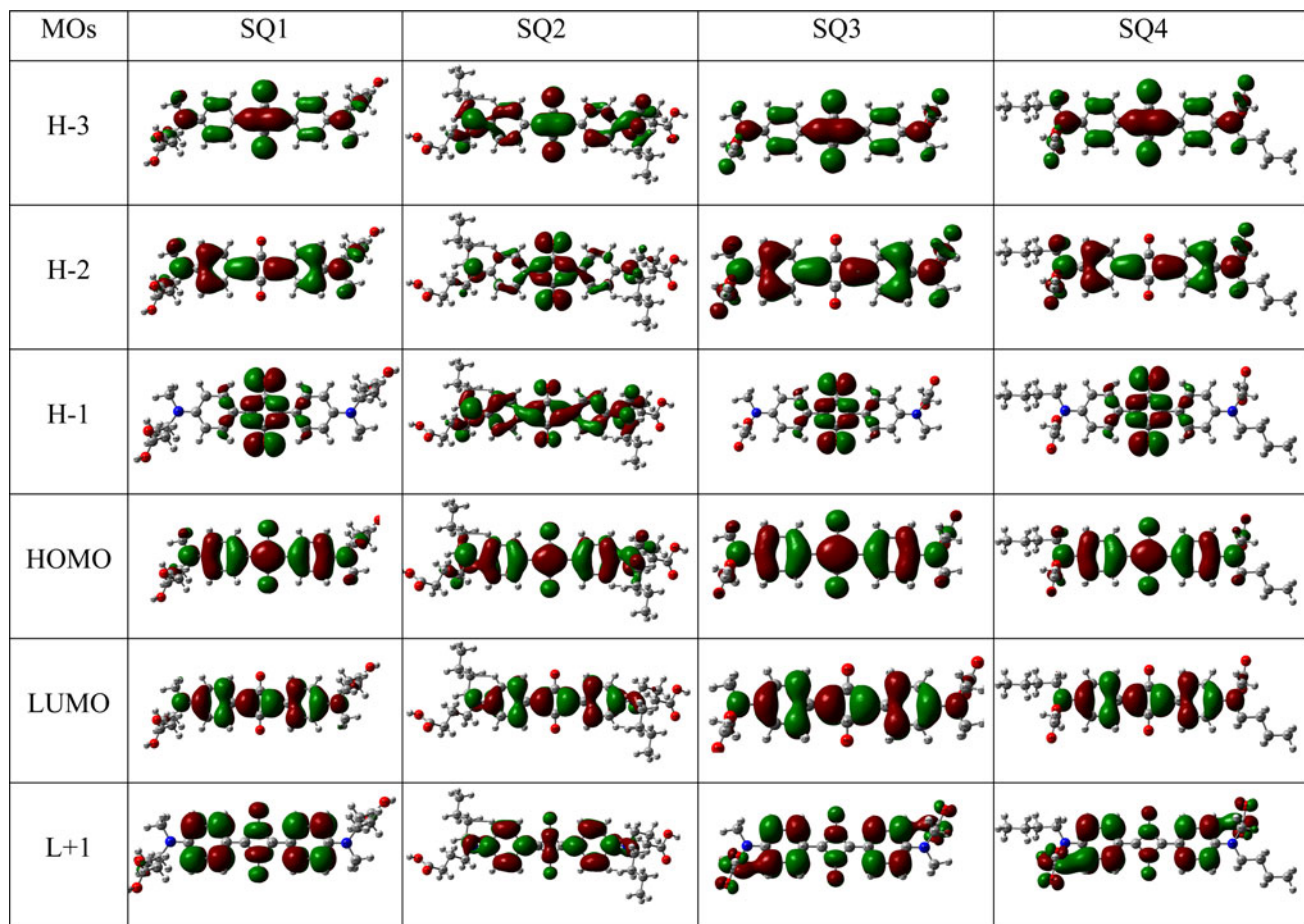


Fig. 3 Isodensity plots (isodensity contour = 0.02 a.u.) of the frontier orbitals of the squaraine dyes SQ1–SQ4

carboxylic group, similar to that of SQ3. The better photoelectric conversion properties of SQ3 and SQ4 than SQ1 and SQ2 could be attributed to the charge flow from the squaraine core to the anchoring groups from the HOMO–LUMO+1 excitation.

The HOMO–LUMO gap of SQ1–SQ4 is 2.23, 2.18, 2.29, 2.26 eV, respectively. The calculated HOMO and LUMO energies of the bare $\text{Ti}_{38}\text{O}_{76}$ cluster as a model for nanocrystallinity are -6.55 and -2.77 eV, respectively, resulting in a HOMO–LUMO gap of 3.78 eV, the lowest transition is reduced to 3.20 eV according to TD-DFT, and this value is slightly smaller than the typical band gap of nm sized TiO_2 nanoparticles [4]. Furthermore, the HOMO, LUMO, and HOMO–LUMO gap of the $(\text{TiO}_2)_{60}$ cluster are -7.52 , -2.97 , and 4.55 eV (B3LYP/VDZ), respectively [24]. Usually an energy gap more than 0.2 eV between the LUMO of the dye and the conduction band of the TiO_2 is necessary for effective electron injection [25]. Taking into account of the cluster size effects and the calculated HOMO, LUMO, and HOMO–LUMO gap for the dyes SQ1–SQ4, and $\text{Ti}_{38}\text{O}_{76}$, and $(\text{TiO}_2)_{60}$ clusters, it can be found that the HOMO energies of these dyes fall within the

TiO_2 gap. The above data also reveal the sensitized mechanism: interfacial electron transfer between semiconductor TiO_2 electrode and the dye sensitizers SQ1–SQ4 are electron-injection processes from excited dyes to the semiconductor conduction band. This is a kind of typical interfacial electron-transfer reaction [26]. Relatively large energy gaps between the LUMO energies of these dyes and the semiconductor conduction band would be beneficial to the photoelectric conversion properties.

Absorption spectra

The UV–vis spectra of the squaraine dyes SQ1–SQ4 were measured in DMSO solution, and have sharp and intense absorption bands with maxima of 651.5, 655.5, 643.0, and 647.5 nm, respectively. In order to understand electronic transitions of SQ1–SQ4, TD-DFT calculations on absorption spectra in DMSO were performed, and the 30 lowest spin-allowed singlet–singlet transitions were taken into account.

The vertical excitation energy and oscillator strength along with the main excitation configuration are listed in

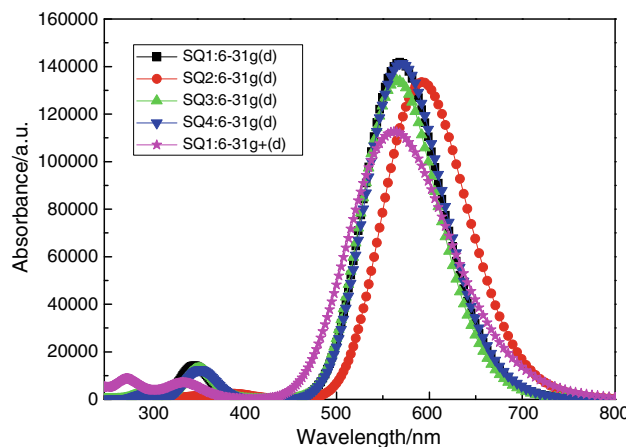


Fig. 4 Simulated absorption spectra of the squaraine dyes SQ1–SQ4

Table 4. The simulated absorption spectra are shown in Fig. 4. It was found that the calculated line shape and relative strength agree well with experimental results. Major electronic absorption bands are assigned to those excitations with significant oscillator strengths. The first optically allowed electronic transitions of SQ1–SQ4 obtained using a 6-31g(d) basis set are predicted to populate the HOMO \rightarrow LUMO transitions at 568.2, 592.2, 565.6, and 570.1 nm, respectively, which have appreciable blue-shifts compared with the experimental absorption maxima. The absorption spectrum of SQ1 was also simulated with a larger 6-31g+(d) basis set; it has an absorption maximum at 561.8 nm and is not significantly different from the results using the 6-31g(d) basis set. Blue-shifted theoretical values are also found for the other squaraine dyes [11, 27, 28], which can be attributed to the inherent approximations in the TD-DFT [29]. The experimental absorption maximum blue-shift of SQ3 and SQ4 with respect to that of SQ1 and SQ2, because the electron-withdrawing ability of the short carboxyl group ($-\text{CH}_2\text{COOH}$) is stronger than the long carboxyl group ($-(\text{CH}_2)_3\text{COOH}$), is well reproduced in our calculation. Therefore, it could be concluded that the TD-DFT calculations are capable of describing the spectral features because of the qualitative agreement of line shape and relative strength with experimental results, although a discrepancy in absorption wavelength exists.

Conclusion

In this paper, the ground-state geometries and electronic structures of symmetrical squaraine dyes SQ1–SQ4 in DMSO were investigated by means of DFT calculations with hybrid functional B3LYP, and the UV–visible spectra were studied by TD-DFT methods. The calculated

Table 4 Computed excitation energies, electronic transition configurations, and oscillator strengths (f) for optical transitions with $f > 0.01$ of the absorption bands in the visible and near-UV regions for the squaraine dyes in DMSO

Dye	Configuration	Excitation energy (eV/nm)	f
SQ1	H \rightarrow L (+72%)	2.18/568.2	1.957
	H-3 \rightarrow L (+89%)	3.57/347.2	0.193
	H \rightarrow L + 1 (+84%)	4.22/293.5	0.030
SQ2	H \rightarrow L (+74%)	2.09/592.2	1.942
	H-3 \rightarrow L (+51%); H-4 \rightarrow L (+39%)	3.19/388.5	0.021
	H-6 \rightarrow L (+88%)	3.55/349.1	0.015
SQ3	H \rightarrow L (+73%)	2.19/565.6	1.852
	H-3 \rightarrow L (+89%)	3.52/352.0	0.177
	H \rightarrow L + 1 (+86%)	4.25/292.0	0.034
SQ4	H \rightarrow L (+73%)	2.17/570.1	1.951
	H-3 \rightarrow L (+89%)	3.51/353.6	0.170
	H \rightarrow L + 1 (+86%)	4.20/295.3	0.033

geometric data indicate that strong conjugation effects occur in the dyes SQ1–SQ4, which is beneficial to intramolecular charge transfer. The HOMO energy levels are calculated to be -4.95 , -5.22 , -5.09 , and -5.06 eV, and the LUMOs are -2.72 , -3.05 , -2.80 , and -2.80 eV for SQ1–SQ4, respectively, indicating that electron transfer from the excited dyes to the TiO_2 conduction band is available. The first optically allowed electronic transitions of SQ1–SQ4 are predicted to populate the HOMO \rightarrow LUMO transition at 568.2, 592.2, 565.6, and 570.1 nm, respectively, blue-shifted compared with the experimental absorption maxima because of the inherent approximations in the TD-DFT.

Computational method

All calculations were performed with the Gaussian 03 software package [30]. The ground-state geometries were fully optimized without any symmetry constraints at the DFT level of theory with Becke's [31] three-parameter hybrid functional and Lee et al.'s [32] correlational functional B3LYP using a standard 6-31g(d) basis set for all atoms. A full NBO analysis was obtained by using the POP = NBO keyword. The excitation energies and oscillator strengths for the lowest 30 singlet–singlet transitions at the optimized geometry in the ground state were obtained in TD-DFT calculations using the same basis set as for the ground state. By using the calculated results, the UV–visible absorption spectra were simulated by a Gaussian convolution with the full width at half-maximum

of 0.4 eV (3,200 cm⁻¹) [4]. Solvation effects were introduced by the SCRF method, via the conductor polarizable continuum model (CPCM) [33, 34] implemented in the Gaussian software, for both geometry optimizations and TD-DFT calculations.

Acknowledgments This work was supported by the Foundation of Wuhan University of Science and Engineering (No. 2009003 and 20073208), the Natural Science Foundation of Hubei Province (No. 2008CDB261), and the Key Project of Science and Technology Research of Ministry of Education (No. 208089). The authors gratefully wish to express their thanks to the reviewers for critically reviewing the manuscript and making important suggestions.

References

- O'Regan B, Grätzel M (1991) *Nature* 353:737
- Nazeeruddin MK, Kay A, Rodicio I, Humphry-Baker R, Müller E, Liska P, Vlachopoulos N, Grätzel M (1993) *J Am Chem Soc* 115:6382
- Nazeeruddin MK, Péchy P, Renouard T, Zakeeruddin SM, Humphry-Baker R, Comte P, Liska P, Cevey L, Costa E, Shklover V, Spiccia L, Deacon GB, Bignozzi CA, Grätzel M (2001) *J Am Chem Soc* 123:1613
- Nazeeruddin MK, Angelis FD, Fantacci S, Selloni A, Viscardi G, Liska P, Ito S, Takeru B, Grätzel M (2005) *J Am Chem Soc* 127:16835
- Gao F, Wang Y, Shi D, Zhang J, Wang M, Jing X, Humphry-Baker R, Wang P, Zakeeruddin SM, Grätzel M (2008) *J Am Chem Soc* 130:10720
- Alex S, Santhosh U, Das S (2005) *J Photochem Photobiol A* 172:63
- Chen Y, Zeng Z, Li C, Wang W, Wang X, Zhang B (2005) *New J Chem* 29:773
- Li C, Wang W, Wang X, Zhang B, Cao Y (2005) *Chem Lett* 34:554
- Otsuka A, Funabiki K, Sugiyama N, Yoshida T, Minoura H, Matsui M (2006) *Chem Lett* 35:666
- Burke A, Schmidt-Mende L, Ito S, Grätzel M (2007) *Chem Comm* 234
- Yum J-H, Walter P, Huber S, Rentsch D, Geiger T, Nüesch F, Angelis FD, Grätzel M, Nazeeruddin MK (2007) *J Am Chem Soc* 129:10320
- Yum J-H, Moon SJ, Humphry-Baker R, Walter P, Geiger T, Nüesch F, Grätzel M, Nazeeruddin MK (2008) *Nanotechnology* 19:424005
- Aiga F, Tada T (2003) *J Mol Struct* 658:25
- Monat JE, Rodriguez JH, McCusker JK (2002) *J Phys Chem A* 106:7399
- Fantacci S, De Angelis F, Selloni A (2003) *J Am Chem Soc* 125:4381
- Angelis FD, Fantacci S, Selloni A (2004) *Chem Phys Lett* 389:204
- Angelis FD, Fantacci S, Selloni A, Nazeeruddin MK (2005) *Chem Phys Lett* 415:115
- Onozawa-Komatsuzaki N, Kitao O, Yanagida M, Himeda Y, Sugihara H, Kasuga K (2006) *New J Chem* 30:689
- Xu Y, Chen W-K, Cao M-J, Liu S-H, Li J-Q, Philippopoulos AI, Falaras P (2006) *Chem Phys* 330:204
- Zhang X, Zhang J-J, Xia Y-Y (2007) *J Photochem Photobiol A Chem* 185:283
- Liu Z (2008) *J Mol Struct (Theochem)* 862:44
- Zhang X, Zhang J-J, Xia Y-Y (2008) *J Photochem Photobiol A Chem* 194:167
- Xu J, Liang G, Wang L, Xu W, Cui W, Zhang H, Li Z (2010) *J Serb Chem Soc* 75:259
- Lundqvist MJ, Nilsing M, Persson P, Lunell S (2006) *Int J Quantum Chem* 106:3214
- Hara K, Kurashige M, Dan-oh Y, Kasada C, Shinpo A, Suga S, Sayama K, Arakawa H (2003) *New J Chem* 27:783
- Watson DF, Meyer GJ (2005) *Annu Rev Phys Chem* 56:119
- Srinivas K, Prabhakar C, Devi CL, Yesudas K, Bhanuprakash K, Rao VJ (2007) *J Phys Chem A* 111:3378
- Feki H, Ahmed AB, Fourati N, Abid Y, Minot C (2009) *J Mol Struct (Theochem)* 895:21
- Champagne B, Guillaume M, Zutterman F (2006) *Chem Phys Lett* 425:105
- Frisch MJ, Trucks GW, Schlegel HB, Scuseria GE, Robb MA, Cheeseman JR, Montgomery JA Jr, Vreven T, Kudin KN, Burant JC, Millam JM, Iyengar SS, Tomasi J, Barone V, Mennucci B, Cossi M, Scalmani G, Rega N, Petersson GA, Nakatsuji H, Hada M, Ehara M, Toyota K, Fukuda R, Hasegawa J, Ishida M, Nakajima Y, Honda Y, Kitao O, Nakai H, Klene M, Li X, Knox IE, Hratchian HP, Cross JB, Bakken V, Adamo C, Jaramillo J, Gomperts R, Stratmann RE, Yazyev O, Austin AJ, Cammi R, Pomelli C, Ochterski JW, Ayala PY, Morokuma K, Voth GA, Salvador P, Dannenberg JJ, Zakrzewski VG, Dapprich S, Daniels AD, Strain MC, Farkas O, Malick DK, Rabuck AD, Raghavachari K, Foresman JB, Ortiz JV, Cui Q, Baboul AG, Clifford S, Cioslowski J, Stefanov BB, Liu G, Liashenko A, Piskorz P, Komaromi I, Martin RL, Fox DJ, Keith T, Al-Laham MA, Peng CY, Nanayakkara A, Challacombe M, Gill PMW, Johnson B, Chen W, Wong MW, Gonzalez C, Pople JA (2004) *GAUSSIAN 03*. Gaussian Inc., Wallingford
- Becke AD (1993) *J Chem Phys* 98:5648
- Lee C, Yang W, Parr RG (1988) *Phys Rev B* 37:785
- Cossi M, Barone V, Cammi R, Tomasi J (1996) *Chem Phys Lett* 255:327
- Barone V, Cossi M (1998) *J Phys Chem A* 102:1995